Neuro-Oncology
27(9), 2265–2280, 2025 | https://doi.org/10.1093/neuonc/noaf107 | Advance Access date 22 April 2025

Therapy-induced senescent glioblastoma cells sustain a procancer immune microenvironment by activating DDX58-mediated STAT1 signaling

Zhixing Wang, Yuxin Zhang, Fan Wu, Bojun Qiu, Yiyun Yin, Xinrun Wang, Ruoyu Huang, Xin Zhang, Zhiyan Sun, Wanjun Tang, Zefan Jing, Wei Han, Tao Jiang, Xiaozhong Peng

All author affiliations are listed at the end of the article

Corresponding Authors: Wei Han, PhD, State Key Laboratory of Common Mechanism Research for Major Diseases, Department of Biochemistry & Molecular Biology, Medical Primate Research Center, Neuroscience Center, Institute of Basic Medical Sciences Chinese Academy of Medical Sciences, School of Basic Medicine Peking Union Medical College, Beijing, China (hanwei2012@ibms.pumc.edu.cn); Tao Jiang, MD, Department of Molecular Neuropathology, Beijing Neurosurgical Institute, Capital Medical University; Department of Neurosurgery, Beijing Tiantan Hospital, Capital Medical University, Beijing, China (taojiang1964@163.com); Xiaozhong Peng, PhD, State Key Laboratory of Common Mechanism Research for Major Diseases, Department of Biochemistry & Molecular Biology, Medical Primate Research Center, Neuroscience Center, Institute of Basic Medical Sciences Chinese Academy of Medical Sciences, School of Basic Medicine Peking Union Medical College; State Key Laboratory of Respiratory Health and Multimorbidity; Institute of Laboratory Animal Science, Chinese Academy of Medical Sciences & Peking Union Medical College, Beijing, China (pengxiaozhong@pumc.edu.cn).

Abstract

Background. Depending on the context, therapy-induced cancer cell senescence promotes or inhibits tumor progression and recurrence, but the underlying mechanism and effects on the tumor immune microenvironment are poorly understood.

Methods. Here, we developed senescent glioblastoma cell models in vitro via drug treatment. The protumor function of senescent cells was demonstrated by coinjection of chemotherapy-induced senescent cells with tumorigenic GL261 cells in C57BL/6J male mice. In addition, conditioned medium coculture experiments were used to explore the functions of senescent glioblastoma cells in vitro. Mechanistically, through a CRISPR-Cas9-based screen, we revealed that the RNA-binding protein DDX58 was induced in senescent glioblastoma cells. By combining RNA sequencing and protein mass spectrometry analysis, we observed that STAT1 signaling was activated. Immunoprecipitation experiments were subsequently performed to identify the interaction between DDX58 and STAT1.

Results. We show that glioblastoma cells can enter a senescent state after chemotherapy. In vivo, senescent glioblastoma cells have a tumor-promoting function and reduce survival in male mice. Mechanistically, we found that the RNA-binding protein DDX58 plays an important role in therapy-induced senescent glioblastoma. Inhibition of DDX58 slowed therapy-induced senescence. The activation of DDX58 depends on the accumulation of mitochondrial double-stranded RNA (mtdsRNA) in the cytoplasm via the BAX protein. Moreover, DDX58 promotes the recruitment of tumor-associated macrophages (TAMs) and their M2-like polarization by activating the STAT1-mediated transcription of colony-stimulating factor 1 (CSF1). We also revealed that DDX58 regulates STAT1 at the post-translational level by inhibiting the ubiquitin E3 ligase TRIM21-mediated STAT1 ubiquitination. Compared with temozolomide (TMZ) treatment alone, treatment with fludarabine, which blocks STAT1 signaling, combined with TMZ can more effectively reduce the recruitment of TAMs and delay tumor growth in vivo. Moreover, knockdown of STAT1 enhances the therapeutic effect of TMZ in vivo and prolongs the survival of tumor-bearing male mice.

Conclusion. A critical mechanism for the protumor immune microenvironment mediated by therapy-induced senescent glioblastoma cells, the DDX58-STAT1-CSF1 axis, may be a potential therapeutic avenue for alleviating traditional therapy-induced glioblastoma cell senescence.

Key Points

- Chemotherapy-induced senescent glioblastoma cells are drivers of cancer progression in vivo.
- mtdsRNA-mediated DDX58-STAT1 signaling was activated in chemotherapy-induced senescent glioblastoma cells to promote TAM recruitment.
- Targeting STAT1 improves the therapeutic efficacy of TMZ in vivo.

Graphical Abstract.

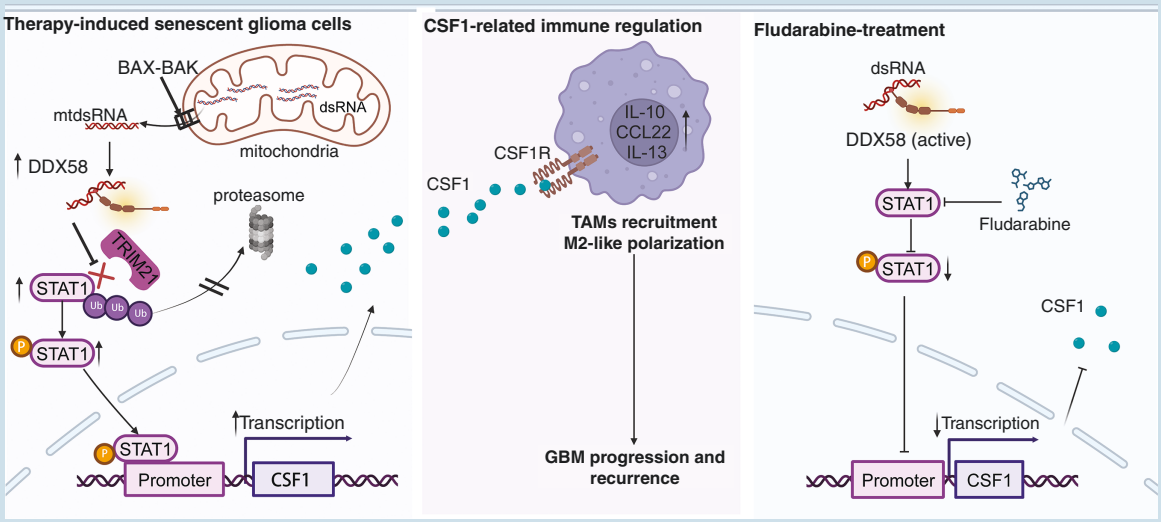

The Role of dsRNA-DDX58-STAT1 Signaling in Glioblastoma Cell Senescence and Macrophage Infiltration: Mechanisms and Therapeutic Implications.

Left panel: Schematic model of the proposed role of dsRNA and DDX58 in regulating the TRIM21-mediated degradation of STAT1 in senescent glioma cells. mtdsRNAs bind to DDX58 and increase its expression. DDX58 increases STAT1 stability by facilitating the dissociation of TRIM21 and STAT1 and then promotes the transcription of CSF1. Middle panel: CSF1 recruits TAMs and enhances their protumor phenotype. Right panel: Fludarabine treatment shows antitumor efficacy by inhibiting STAT1-mediated transcription of CSF1. Abbreviations: mtdsRNA: Mitochondria double-stranded RNA; DDX58: Retinoic acid-inducible gene 1 protein; STAT1: Signal transducer and activator of transcription 1; Ub, ubiquitin; CSF1: Colony stimulating factor 1; TAMs: Tumor-associated macrophages.

Importance of the Study

In different contexts, senescent cancer cells have heterogeneous functions. To avoid the possible side effects mediated by the resulting senescent glioblastoma cells, the functions and mechanisms of senescent glioblastoma cells were characterized in this study. Here, we revealed that chemotherapy-induced senescent glioblastoma cells have a tumor-promoting function and reduce survival in male mice. We also showed that chemotherapy-induced glioblastoma cell senescence promotes TAM recruitment via mtdsRNA-mediated activation of DDX58-STAT1 signaling, leading to tumor progression. Inhibiting STAT1 in combination with TMZ treatment has a better therapeutic effect in vivo. These findings will help improve traditional anti-tumor treatment strategies.

Glioblastoma (GBM) is the most aggressive and lethal brain cancer. The standard-of-care therapy method for primary GBM is maximal surgical resection followed by temozolomide (TMZ) chemotherapy and radiation therapy.[1] However, patient benefit from the standard strategy is very limited. The majority of patients relapse within a short period of time. Many factors can contribute to poor benefit and GBM recurrence, including drug resistance of inherent cancer cells and glioma stem-like cells, tumor dormancy and tissue factor-mediated remodeling of the immune microenvironment.[2–6] GBM contains a highly immunosuppressive tumor microenvironment (TME) that promotes tumor progression and resistance to therapy,[7] and the high abundance of tumor-associated macrophages (TAMs) may be a key factor in glioblastoma immunosuppression.[8] TAMs have phenotypic and functional plasticity, and can be activated toward either a "classic (M1)" or an "alternative (M2)" phenotype.[9] M1-type macrophages produce proinflammatory molecules, such as tumor necrosis factor alpha (TNF-α), which inhibit tumor growth and support T-cell activity.[8,10] In addition, M2 macrophages inhibit T-cell functions and inflammatory TAM activities and promote tumor progression.[11,12] Glioma cells can attract TAMs by secreting many factors, which in turn enhance immunosuppression, mainly through their transformation into M2-type macrophages.[13,14] Therefore, blocking the connection between TAMs and related cells may also be a novel therapeutic strategy to mitigate GBM progression and recurrence.

For the past several decades, researchers have suggested that cellular senescence is primarily a physiological response that occurs in normal somatic cells and is an anticancer mechanism.[15–17] However, recent studies have shown that tumor cells also undergo senescence, and that senescent tumor cells (STCs) specifically inhibit or promote tumor progression and recurrence, which is different from physiological senescence.[18–21] On the one hand, tumor cell growth is halted by senescence. On the other hand, STCs may remodel the TME to promote or inhibit tumorigenesis and progression through the heterogeneous SASPs.[22] Previous studies have revealed that STCs can enhance immunosurveillance and promote antitumor immunity by activating dendritic cells and antigen-specific CD8 T cells.[20] However, other studies have reported that some STCs can mediate protumorigenic effects by secreting SASPs, to promote the collective invasion of cancer cells and inhibit CD8 T-cell infiltration.[18] In addition, recent in vivo evidence suggests that the removal of senescent malignant cells can hinder tumor progression and improve survival by modifying the tumor ecosystem in GBM.[23] Similarly, another study showed that radiation therapy promotes the production of SA-βGal + GBM cells and orchestrates an immunosuppressive TME by activating TAMs.[24] Together, these studies suggest that senescent tumor cells could be a key factor in promoting GBM oncogenesis and leading to recurrence. Regrettably, the role and mechanisms underlying chemotherapy-induced senescent tumor cell remodeling in the GBM immune microenvironment remain unclear.

Here, we used multiomic data integration, including a CRISPR-Cas9–based loss-of-function screen at the genomic level and combined transcriptome and proteome analyses of senescent LN229 cells, to reveal the targetable mechanisms by which senescent glioma cells promote GBM progression and recurrence. Furthermore, a senescence-targeted therapy was proposed on the basis of traditional therapy, which can potentially be used in preclinical and clinical adjuvant GBM therapy.

Materials and Methods

Ethics Statement

The related studies were approved by the institutional review board of Institute of Basic Medical Sciences, Chinese Academy of Medical Sciences (ZS2023007). All the animal studies were approved by the Institutional Animal Care Use & Welfare Committee of the Center for Experimental Animal Research (ACUC-A01-2022-059, ACUC-A02-2025-005).

Cell lines, in vitro culture and lentivirus

Patient-derived GBM cells (PDCs) lines T3-5, human LN229, U87MG and murine GL261 glioma cells were used in these studies. Lentiviruses were purchased from Shanghai Genechem.

Intracranial tumor models and drug treatment

Male or Female C57BL/6J mice (5–6 weeks of age) were selected for the establishment of in vivo mouse models. GL261-luc cells or senescent GL261-luc cells were injected into the mouse brain. The mode of drug administration and concentration of drugs used for treatment are described in the figures. Luciferase-expressing tumors were monitored via the Xenogen IVIS.

β-galactosidase staining

GBM cell senescence was induced by treatment with TMZ or DOX. The cells were stained for β-galactosidase activity via a SA-β-Gal Stain Kit (Solarbio, G1580).

Immunoblot

Immunofluorescence, flow cytometry and western blot were performed in brain tissues and GBM cells. Antibodies are listed in Supplementary Table S3.

CRISPR screening

LN229 cells were infected with lentiviruses carrying the pooled CRISPR knockout library. The cells were subsequently frozen for genomic DNA extraction and Illumina sequencing. The results were analyzed via MAGeCK.

High-Throughput sequencing and qRT-PCR

RNA-seq and mass spectrometry analysis were performed in LN229 and senescent LN229 cells. Total RNA was

extracted from GBM cells and senescent cells via the TRIzol reagent (Invitrogen, Carlsbad, State of California, USA). qRT-PCR analyses were performed on a CFX96 Real-Time PCR Detection System (Bio-Rad). All the qPCR primers used are listed in Supplementary Table S4.

ChIP–qPCR

Chromatin immunoprecipitation was performed using a Pierce Magnetic ChIP Kit (Thermo Scientific, 26157). The DNA was purified via a DNA Clean-Up Column and verified via qPCR. The sequences of the primers used for ChIP–qPCR are listed in Supplementary Table S4.

Plasmid construction and siRNA transfection

The pcDNA3.1 and pcDNA4.0 Plasmids were constructed via a ClonExpress MultiS One Step Cloning Kit (Vazyme C113). siRNAs were purchased from Gene Pharma Corporation, and the sequences are listed in Supplementary Table S4.

Conditioned media and enzyme-linked immunosorbent assay (ELISA)

Conditioned media were prepared from the cell supernatants of GBM cells. Secreted CSF1/M-CSF protein levels were measured via a human macrophage colony-stimulating factor (M-CSF) ELISA kit (CUSABIO CSB-E04658h).

Luciferase reporter assay

Luciferase reporter assay were performed on a dual-luciferase reporter assay system (Promega, Madison, WI, USA). See Supplementary Materials and Methods for the details

dsRNA-protein immunoprecipitation

dsRNA-protein immunoprecipitation were performed in LN229 cells. For details see Supplementary Materials and Methods.

Single-cell RNA-seq data analysis

Two datasets GSE190129 and GSE226468 were analyses in R software. See Supplementary Materials and Methods for the details of process.

Statistical analysis

The statistical analyses were performed via GraphPad Prism 7.0 software. For details see Supplementary Materials and Methods.

See Supplementary Materials and Methods for detailed experimental procedures.

Data availability

Two single-cell sequencing (scRNA-seq) datasets were obtained from the Gene Expression Omnibus database under the accession codes GSE190129 (human GBM cells) and GSE226468 (mouse TME). The data underlying Figures 4 and S4 are available in the Supplemental Tables.

Results

Therapy induced senescence-like features in glioblastoma cells in vivo.

To investigate the features of temozolomide-induced senescent GBM cells in vivo, a single-cell sequencing (scRNA-seq) dataset from a patient-derived tumor xenograft (PDX) model was used to analyze the status of GBM cells after TMZ treatment.[25] Uniform manifold approximation and projection (UMAP) clustering at 0.4 resolution identified cancer, astrocyte, oligodendrocyte, and neuron as 4 distinct lineages with distinct gene expression signatures in PDX samples, including two samples treated with TMZ and eight untreated samples (Figure 1A-1B). We then applied the AUCell senescence score based on three senescence and two SASP gene sets (Supplementary Table S1). The results revealed that the senescence and SASP signature score was increased in cancer and astrocyte cells (Figure 1C-1D and S1A). We assessed the expression of *CDKN1A*, *IGFBP4*, *IGFBP7*, *F3* and *NFE2L2* previously described as upregulated in cancer cells (Figure 1E). In addition, we used another mouse scRNA-seq dataset to analyze TME components after TMZ treatment.[26] UMAP clustering of $Cd45^{+}Cd11b^{+}$ cells identified bone marrow-derived macrophages (BMDM) and microglia as 2 distinct clusters (Figure S1B). We observed increased expression of *Cd68*, *Spp1* and *Iba1* genes in BMDM and *P2ry12*, *Tmem119* in microglia cells (Figure 1F and S1C). To further clarify the effect of TMZ on the induction of senescence, we used GL261 cell-driven intracranial models in C57BL/6J mice. The models with tumors were treated with TMZ for 7 days. (Figure 1G). The results indicated that tumor growth was significantly inhibited (Figure S1D). The expression of Cdkn1a (p21) and Cdkn2a (p16) was increased, whereas that of Lmnb1 was decreased by TMZ treatment in vivo (Figure S1E). Furthermore, after TMZ treatment, we detected an increase in SPP1-, ARG1-, IBA1-positive cells (Figure 1H-1I). However, the number of microglial cells does not appear to show significant changes (Figure S1F-S1G). Flow cytometric analysis revealed that the proportion of $F4/80^{+}Cd68^{+}$ and $F4/80^{+}Cd163^{+}$ myeloid cells increased after TMZ treatment (Figure S1H).

Coinjection of senescent glioblastoma cells with tumorigenic cells promoted senescence-associated tumor growth in vivo

To evaluate the impact of senescent GBM cells on tumor progression in vivo, we generated GL261 murine-derived senescent GBM cells in vitro. GL261 cells were treated with 300 μM TMZ for 5 days or 100 nM DOX for 3 days and

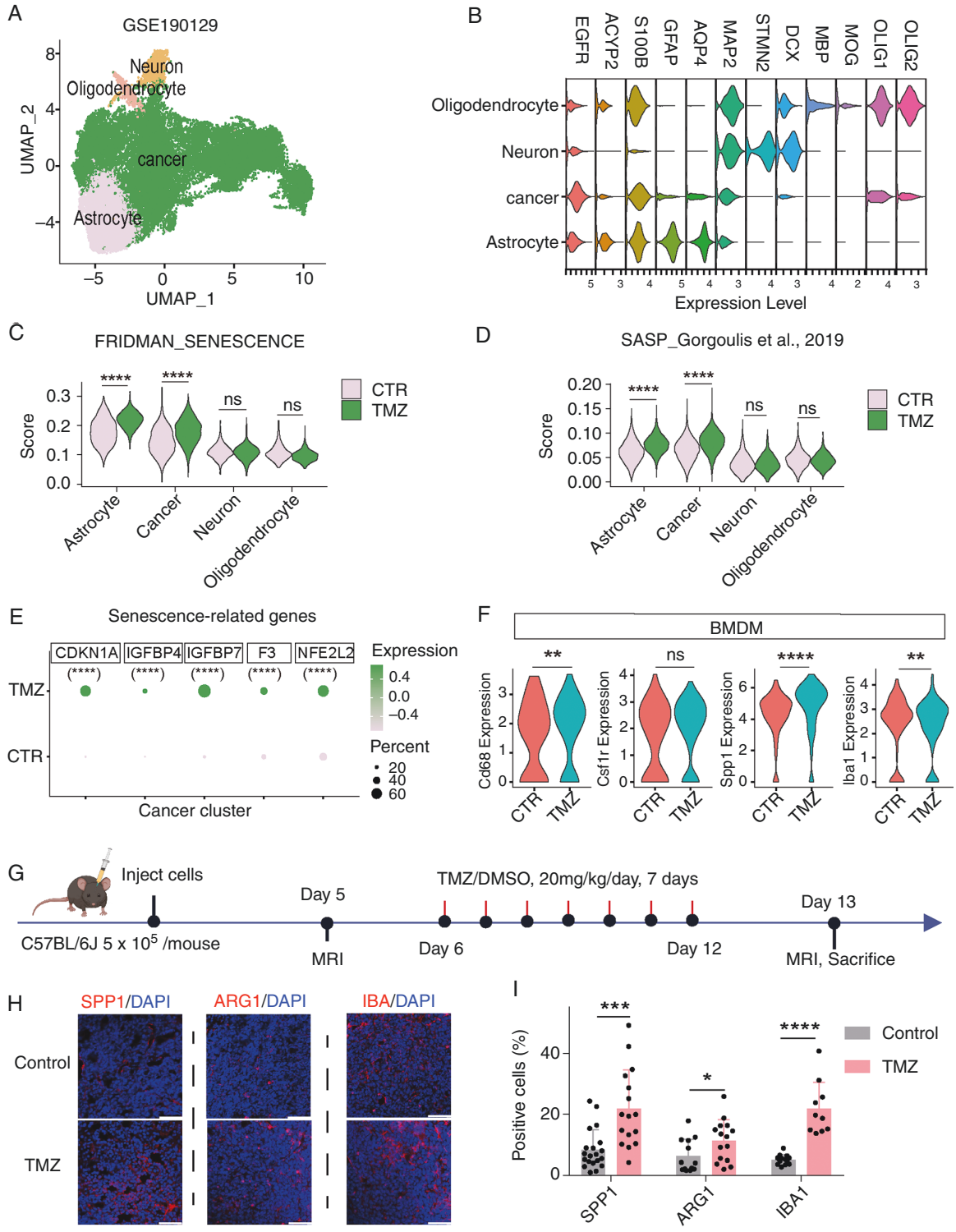

Figure 1. Therapy induced senescence-like features in glioblastoma cells and alterated the immune compartment in vivo (**A**). UMAP plot showing cell types from patient tumors. (**B**). VlnPlots of the expression of glioma cell, oligodendrocyte, neuron and astrocyte cell markers in patient tumors. (**C-D**). VlnPlots of the difference of FRIDMAN_senescence and SASP score in patient tumors from the CTR- and TMZ-treated groups. $^{****}p < 0.0001$ by two-tailed unpaired Student's t test (**E**). DotPlot of the expression of senescence-related genes. $^{****}p < 0.0001$ by two-tailed unpaired Student's t test. (**F**). VlnPlots of the expression of Cd68, Csf1r, Spp1 and Iba1in BMDM clusters. $^{**}p < 0.01$, $^{****}p < 0.0001$ by two-tailed unpaired Student's t test. (**G**). In vivo efficacy studies of TMZ in C57BL/6J mouse models with intracranial tumors. GL261 cells were implanted into the mouse brain, and the strategy is shown. (**H-I**). Immunofluorescence staining and quantitative analysis of SPP1, ARG1 and IBA1 revealed the TAM and M2-like macrophage contents on Day 13. Scale bars, 50 μm. All the samples were analyzed in 3–5 fields per slice. $^{*}p < 0.05$, $^{***}p < 0.001$ and $^{****}p < 0.0001$ by one-way ANOVA with Tukey's multiple comparison test. All the data are presented as the means ± SDs.

then stained with the CellEvent Senescence Green Probe. The results revealed that SA-βGal activity (Figure S2A) and the expression of several SASP genes (Figure S2B) and P21 increased (Figure S2C). Then, we coinjected senescent GL261 cells with proliferative GL261 cells, which express luciferase, into the intracranial region of C57BL/6J male or female mice (Figure 2A). When equal proportions of GL261-luc cells (2.5×10^5) and senescent GL261-luc cells (2.5×10^5) were coinjected (Group 3), tumor growth was promoted in male mice (Figure 2B). In contrast, senescent cells did not promote tumor growth in female mice (Figure S2D-S2F). Flow cytometric analysis revealed that the proportion of myeloid cells was greater in Group 3 than in the control group (Group 1) in male mice (Figure 2C-2D). Furthermore, $ARG1^+$ and $IBA1^+$ macrophages were markedly increased in Group 3 tumors of male mice (Figure 2E-2F). However, senescent GBM cells exhibited no significant effect on myeloid and macrophage infiltration within the female TME (Figure S2G-S2I). Furthermore, male mice in Group 3 and Group 2 exhibited more rapid body weight reduction compared to Group 1(Figure 2G). Most importantly, the presence of senescent GBM cells significantly decreased the survival of GBM-bearing mice compared with that of control (Group 1) in male mice (Figure 2H). These data suggest a potential relationship among senescent GBM cells, tumor progression, and TAM infiltration.

Senescent glioblastoma cells promoted TAM migration and M2-like polarization in vitro

To validate the function of senescent GBM cells in vitro, LN229, U87MG and T3-5 cells were treated with TMZ or DOX, which resulted in an increase in SA-βGal activity (Figure 3A-3B), P21 upregulation (Figure 3C), Lamin B1 protein downregulation (Figure 3C) and SASP genes upregulation (Figure 3D). In addition, the presence of TMZ or DOX triggered a significant decrease in Ki-67 staining in Figure S3A-S3B. Further experimental results revealed that after treatment with TMZ or DOX, the cell-cycle was arrested (Figure S3C-S3D).

To clarify whether senescent GBM cells promote TAM migration, the conditioned medium of senescent cells was cocultured with phorbol myristate acetate (PMA)-induced THP-1 macrophages. When conditioned media (CM) from TMZ- or DOX-induced senescent GBM cells were placed in the lower chamber, more macrophages migrated from the upper to the lower chamber (Figure 3E-3I). To explore whether senescent tumor cells affect macrophage polarization, we directly cocultured PMA-induced THP-1 macrophages with CM from proliferating LN229 cells or TMZ-induced senescent LN229 cells. The THP-1 macrophages differentiated into M2-like macrophages in CM from senescent LN229 cells presented increased expression of mRNAs associated with M2-like macrophages (Figure S3E). However, the expression of mRNAs associated with M1-like macrophages was not significantly increased (Figure S3F). Taken together, these data further suggest that chemotherapy-induced senescent GBM cells influence the recruitment and polarization of macrophages, resulting in a cancer-supportive environment.

CRISPR-Cas9-based screening for senescence-related RNA-binding proteins in glioblastoma cells

Senescent cells play critical roles in aging and age-related diseases, including cancer.[27] RNA-binding proteins are involved in the regulation of cellular senescence, mainly at the post-transcriptional level.[28] To clarify the function of RBPs in senescent GBM cells, we performed a CRISPR-Cas9–based loss-of-function screen in a senescent LN229 cell model via a pooled human CRISPR knockout library targeting 1136 RNA-binding protein-coding genes. We exposed the transduced LN229 cells to 50 μM TMZ for 4 and 8 days or 100 nM DOX for 3 and 6 days, after which the cells at specific time points were collected for deep sequencing (Figure 4A). Compared with that of the untransduced cells, the percentage of SA-βGal–negative cells increased after treatment (Figure S4A). This result indicated that the CRISPR-Cas9–mediated disruption of certain RBP genes alleviates LN229 cell senescence. We performed sgRNA sequencing on LN229 cells collected on Day 0, Day 4 (TMZ treatment), Day 8 (TMZ treatment), Day 3 (DOX treatment), and Day 6 (DOX treatment). We then analyzed the sgRNAs that were positively enriched at Days 3, 4, 6, and 8 relative to Day 0. These positively enriched genes may serve as potential regulators of cellular senescence (Figure 4B). TP53, a well-established senescence related gene, and SASP-regulating gene,[29] was significantly enriched after TMZ or DOX induction (Figure 4B) and was used as a positive control in our screening system. Interestingly, based on the lower *P*-value, the double-stranded RNA-binding protein DDX58 was identified as one of the top targets in both positive screens (Figure 4B). To determine the role of DDX58 in GBM cell senescence, we used small interfering RNAs targeting DDX58 in LN229 cells, and siDDX58-2 and siDDX58-3 resulted in highly efficient depletion (Figure S4B). The expression of the senescence marker P21 and the activity of SA-βGal decreased when DDX58 was depleted in senescent LN229 cells (Figure 4C and S4C-S4D). Together, these results indicate that RBP DDX58 deficiency alleviates the senescence phenotypes of chemotherapy-induced senescent LN229 cells.

Next, we performed RNA sequencing and protein mass spectrometry analysis of TMZ- or DOX-treated LN229 cells to determine the pathways that may be affected in these cells. The results of differential gene expression analysis revealed 2700 upregulated genes and 1171 downregulated genes in senescent LN229 cells under treatment with TMZ, which was a 1.5-fold change (Figure S4E). Gene Ontology (GO) and Reactome pathway enrichment analyses revealed a number of enriched pathways, including cell division, regulation of the cell cycle, interferon and cytokine-related signaling in the immune system (Figure S4F-S4G, Supplementary Table S1). Similarly, gene set enrichment analysis (GSEA) of TMZ-induced senescent LN229 cells compared with proliferating cells revealed downregulation of the mitotic-related pathways and upregulation of pathways involved in immune regulation (cytokine signaling, interferon responses, and interleukin 10 signaling) (Figure S4H). Moreover, GSEA revealed significant upregulation of the senescence and SASP gene sets (Figure 4D). By analyzing the proteome, we identified 1504 differentially

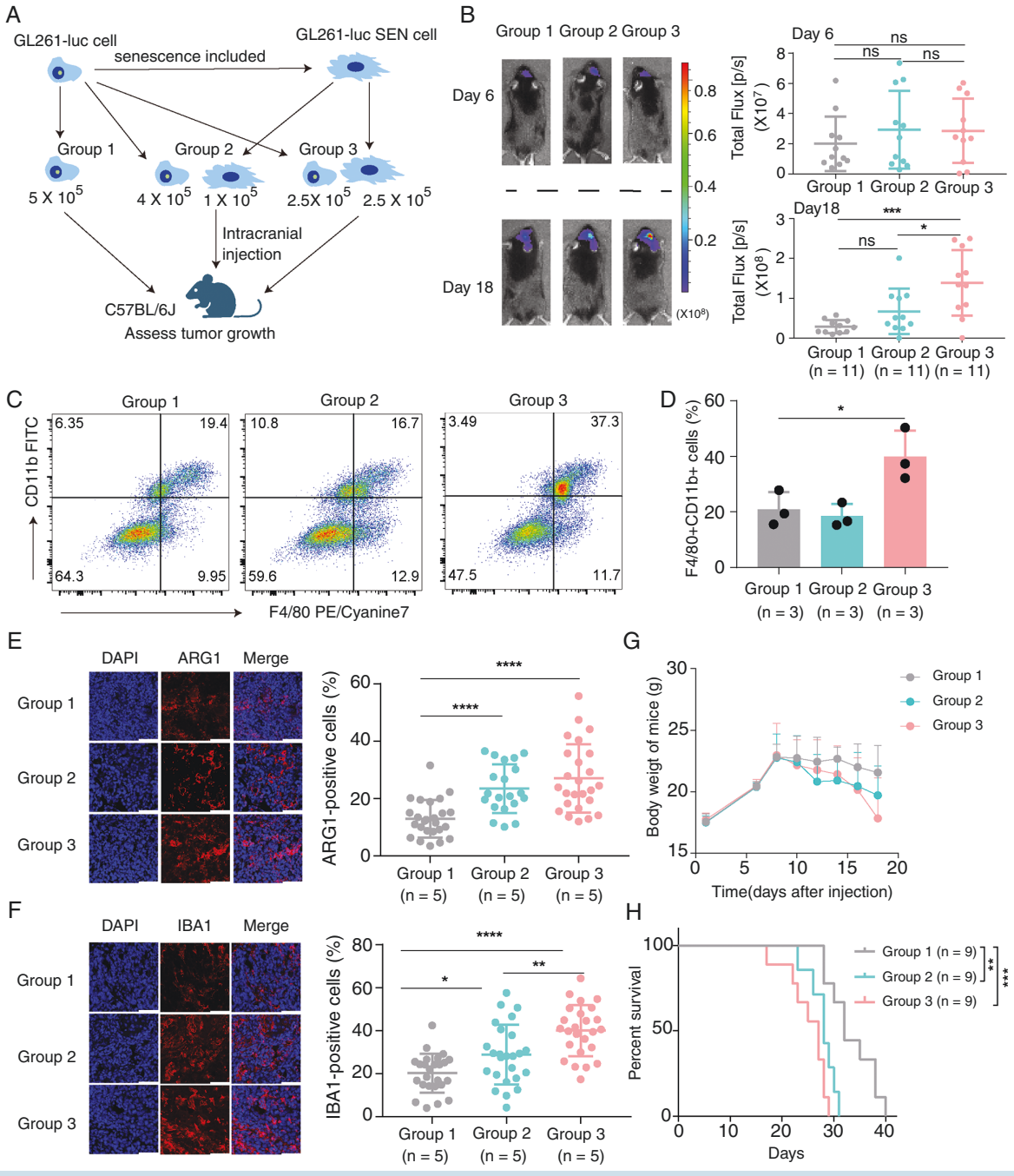

Figure 2 . Coinjection of senescent glioma cells with tumorigenic cells promoted tumor growth in vivo. (**A**). Scheme of the coinjection of senescent GL261-luc glioma cells with tumorigenic cells. (**B**). Images of the fluorescent signal from GL261-luc cells injected alone or coinjected with GL261 cells and senescent GL261 cells were obtained via the Q-Lumi in Vivo imaging system. Graph representing the integrated density over time from independent tumors. The data are presented as the means ± SDs of n = 11 tumors (Group 1: GL261-luc alone), n = 11 tumors (Group 2), and n = 11 tumors (Group 3). Box and whisker plots representing the integrated density at 6 and 18 days postimplantation. The data are the means ± SDs. *$p < 0.05$ and ***$p < 0.001$ by one-way ANOVA with Tukey's multiple comparison test. (**C-D**). Proportion of F4/80 + Cd11b + myeloid cells in tumors. The data are the means ± SDs. *$p < 0.05$ by one-way ANOVA with Tukey's multiple comparison test. (**E-F**). Immunofluorescence staining and quantitative analysis of ARG1 and IBA1 revealed the TAM and M2-like macrophage contents on Day 18 postimplantation. Scale bars, 50 µm. All the samples were analyzed in 3–5 fields per slice. "n" indicates the number of samples. The results are presented as the means ± SDs. *$p < 0.05$ and ****$p < 0.0001$ by one-way ANOVA with Tukey's multiple comparison test. (**G-H**). The mouse body weights are shown in (G). The survival curves are shown in (H). The Mantel–Cox log–rank test was used for analysis, **$p < 0.01$ and ***$p < 0.001$.

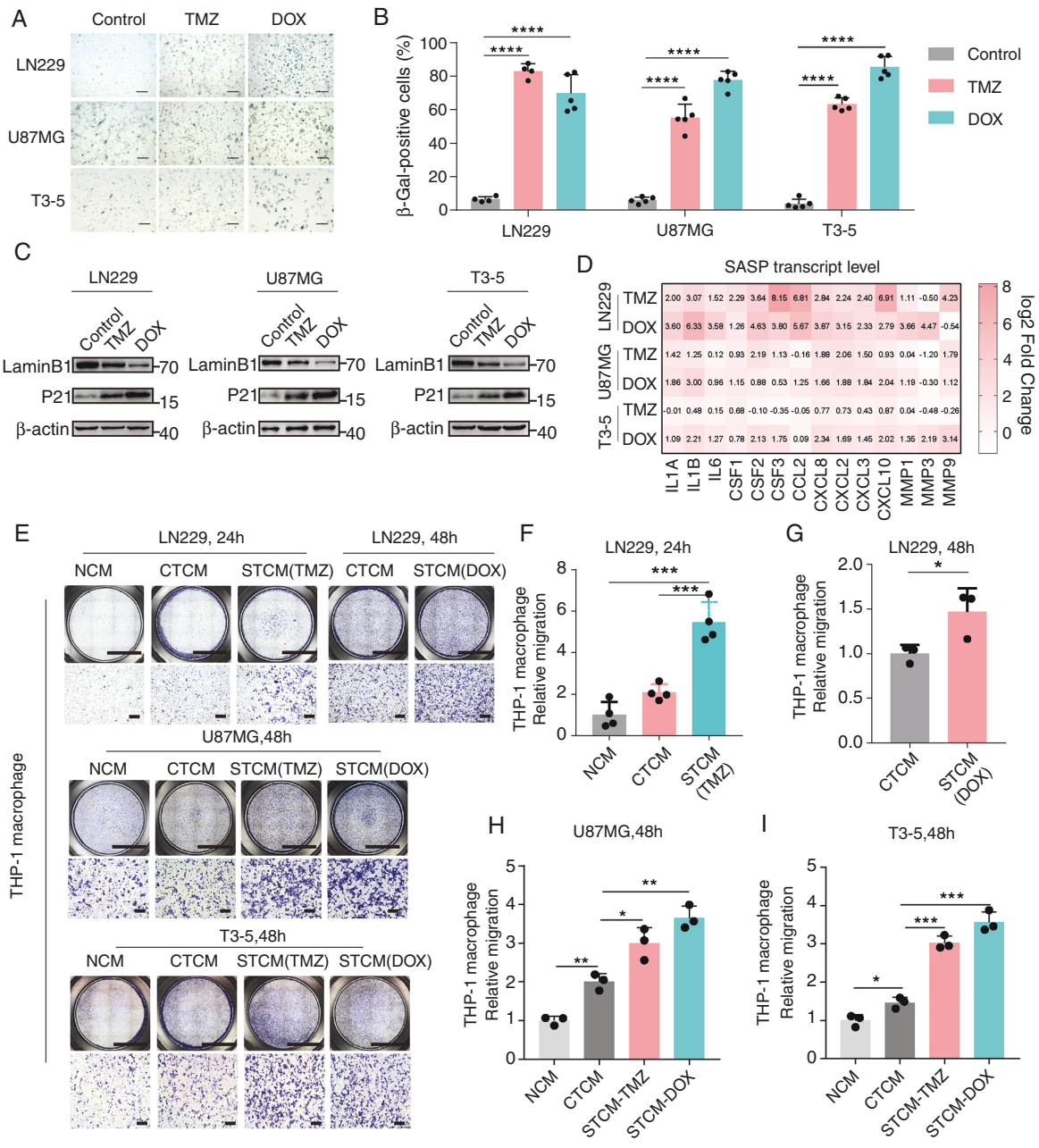

Figure 3. Senescent GBM cells promoted TAM migration in vitro. (**A**).SA-β-gal was assessed via X-gal staining in LN229 treated with 50 μM TMZ for 5 days and 100 nM DOX for 3 days, U87MG cells treated with 100 μM TMZ for 5 days and 100 nM DOX for 3 days and in T3-5 cells treated with 300 μM TMZ for 5 days and 100 nM DOX for 3 days. Scale bar, 100 μm. (**B**). Quantitative analysis of SA-β-gal-positive LN229, U87MG and T3-5 cells after TMZ or DOX treatment. All the data are presented as the means ± SDs. $^{****}p < 0.0001$ by one-way ANOVA with Tukey's multiple comparison test. (**C**). Western blot analysis of Lamin B1 and P21 proteins in LN229, U87MG and T3-5 cells. (**D**). Heatmaps depicting real-time qPCR analysis of mRNA expression of indicated SASP genes in senescent LN229, U87MG and T3-5 cells. (**E-I**). THP-1 macrophages were cocultured with CM (200 μg/mL) from LN229 cells (NCM, no conditioned media; CTCM, conditioned medium from proliferating cells; and STCM, conditioned medium from senescent cells) for 24 h or 48 h, and THP-1 macrophage migration was analyzed (F-G) via ImageJ and GraphPad Prism. The lower panel shows images of the transwell assay. Scale bars: 2 mm, 100 μm. The data were analyzed in triplicate. The three groups were compared via one-way ANOVA with Tukey's multiple comparison test. $^{*}p < 0.05$, $^{***}p < 0.001$. THP-1 macrophages were cocultured with CM (200 μg/mL) from U87MG or senescent U87MG cells, and the results were statistically analyzed (H). $^{**}p < 0.01$ by one-way ANOVA with Tukey's multiple comparison test. Scale bars: 2 mm, 100 μm. THP-1 macrophages were treated with CM (200 μg/mL) from T3-5 or senescent T3-5 cells, and the results were statistically analyzed (I). $^{*}p < 0.05$ and $^{***}p < 0.001$ by one-way ANOVA with Tukey's multiple comparison test. Scale bars: 2 mm, 100 μm.

expressed proteins with a 1.5-fold change, including 901 upregulated and 603 downregulated proteins, in TMZ-treated senescent LN229 cells (Figure S4I, Supplementary Table S2). GO and pathway analysis revealed that genes related to the regulation of transcription, the innate immune response and cell division were enriched (Figure S4J-S4K).

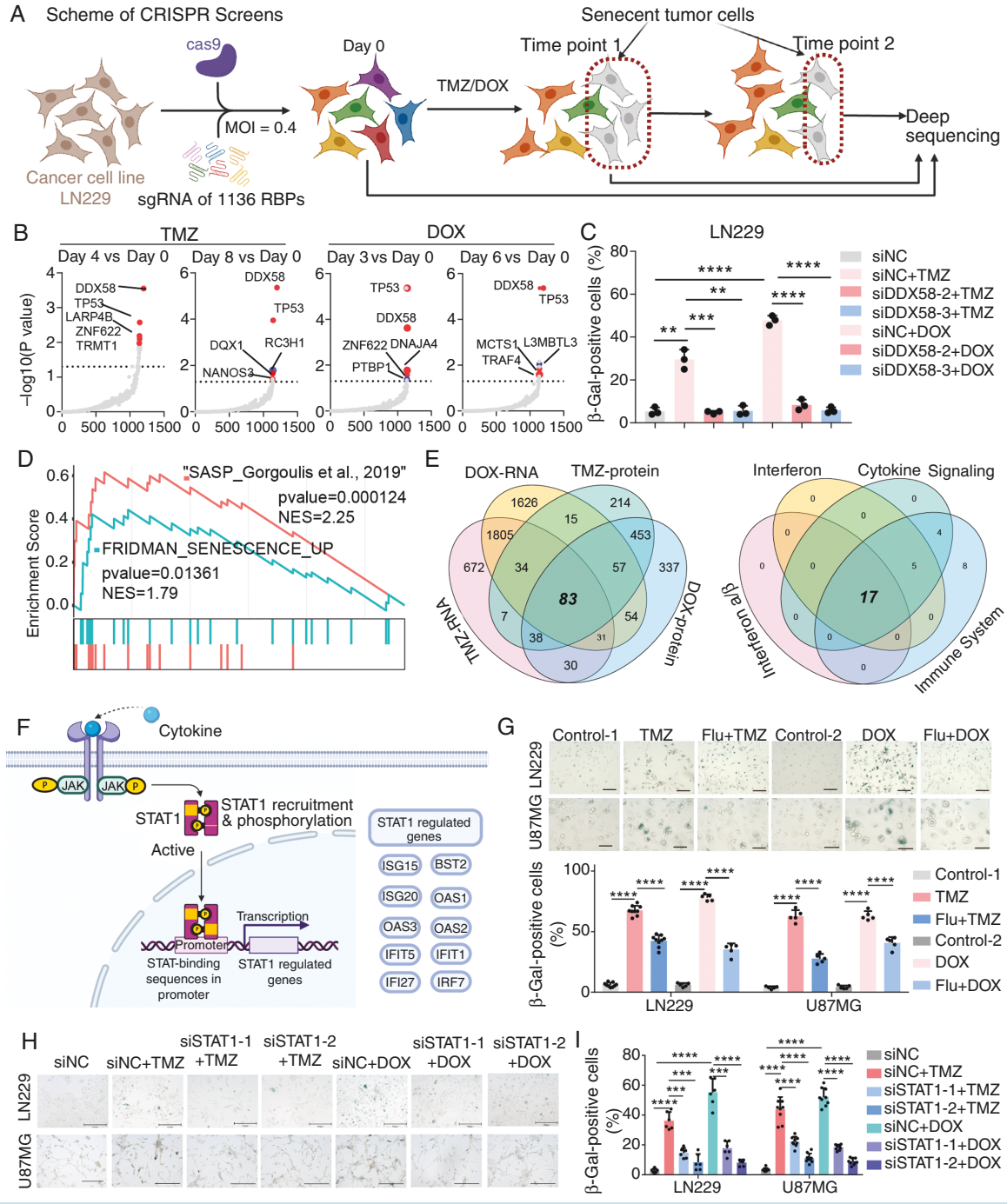

Figure 4. CRISPR-Cas9-based screen and high-throughput sequencing identifies senescence related genes and pathways (**A**). Schematic diagram illustrating the workflow of CRISPR/Cas9 knockout library screening. (**B**) The enrichment score was calculated for each gene on the basis of its prevalence in the pool of 50μM TMZ-treated LN229 cells harvested at 4 and 8 days and 100nM DOX-treated cells harvested at 3 and 6 days after viral infection relative to Day 0. The genes detected in the library are shown as dots in the diagram; the red dots indicate some of the top 5 enriched genes in each positive screen. (**C**). Graph showing the percentage of SA-βgal-positive cells. The data are presented as the means of three biological replicates ± SDs. $^{**}P < 0.01$, $^{***}P < 0.001$, $^{****}P < 0.0001$ by two-tailed unpaired Student's t test. (**D**). GSEA graphs of RNA-seq data from TMZ-induced senescent LN229 cells compared with untreated cells. The FRIDMAN_Senescence_UP and SASP gene lists are shown in Supplementary Table S1. (**E**) A venn plot of upregulated genes and proteins (with greater than a 1.5-fold change) across the RNA sequencing and mass spectrometry data. And the venn plot of shared genes or proteins across four immune-related pathways. (**F**). The STAT1-related genes and proteins were manually mapped from (E) via BioRender.com. (**G**). SA-βgal staining of LN229 and U87MG cells. The corresponding treatment conditions were as follows. LN229 cells, TMZ: 50 μM for 4 days, DOX: 100 nM for 3 days, Flu + TMZ: 1 μM fludarabine for 24 h followed by 50 μM TMZ for 4 days, Flu + DOX: 1 μM fludarabine for 24 h followed by 100 nM DOX for 3 days. U87MG cells, TMZ: 100 μM for 5 days, DOX: 100 nM for 3 days, Flu + TMZ: 1 μM fludarabine for 24 h followed by 100 μM TMZ for 5 days, Flu + DOX: 1 μM fludarabine for 24 h followed by 100 nM DOX

for 3 days. Quantitative analysis of the data in the graph represents % SA-βgal-positive cells. The samples were analyzed with 5–9 fields per well. ****$p < 0.0001$; one-way ANOVA with Tukey's multiple comparison test. Scale bar, 100 μm (**H**). SA-βgal staining of STAT1-depleted LN229 and U87MG cells treated with TMZ or DOX. Scale bar, 200 μm. (**I**). Graph showing the percentage of SA-βgal positive LN229 and U87MG cells. ***$p < 0.001$, ****$p < 0.0001$; one-way ANOVA with Tukey's multiple comparison test.

Next, we intersected genes that were upregulated by at least 1.5-fold at both the RNA and protein levels, identifying 83 genes. We then performed pathway enrichment analysis on these 83 upregulated genes and found four immune-related signaling pathways to be significantly enriched. By intersecting the differentially expressed genes covered by these four pathways, we identified 17 genes that were upregulated in immune-related pathways (Figure 4E, Supplementary Table S2). We then manually mapped 17 molecules, 10 of which were downstream of STAT1 (Figure 4F). These results suggest that STAT1-mediated immune-related signaling may play an important role in senescent GBM cells.

Fludarabine impeded glioma cell senescence and SASP gene expression by inhibiting STAT1 signaling

To further validate the function of STAT1 in senescent cells, we pretreated LN229 and U87MG with fludarabine (Flu), a STAT1 inhibitor. We subsequently induced pretreated glioma cells via TMZ or DOX. Notably, fludarabine pretreatment inhibited the upregulation of the STAT1 protein in senescent LN229 and U87MG cells (Figure S5A-S5B). The qPCR results revealed that the expression of several STAT1- and SASP-related genes, including *CSF1*, was decreased in the Flu plus TMZ group of LN229 and U87MG cells (Figure S5C-S5F). Compared with those in the senescent group (TMZ or DOX alone), the number of SA-βGal–positive cells was lower in the fludarabine (1 μM) pretreatment (Flu plus TMZ or DOX) group (Figure 4G). In GBM, TAMs depend on CSF-1 for differentiation and survival by binding CSF-1 receptor (CSF-1R).[30] Using the cistrome data browser database, we found that STAT1 has a relatively specific binding peak in the promoter of *CSF1* (Figure S5G). STAT1 inhibition abolished the binding of STAT1 around the CSF1 promoter region (Figure S5H). In addition, TMZ or DOX treatment increased luciferase activity in LN229 cells containing the CSF1 promoter (Figure S5I). ELISA analysis revealed that the secretion of CSF1 protein was increased in senescent LN229 cells (Figure S5I). To further determine the role of STAT1 in cellular senescence, we used two small interfering RNAs targeting STAT1 in LN229 cells (Figure S5J). We observed that depleting STAT1 from LN229 and U87MG cells inhibited their ability to commit to the senescent phenotype (Figure 4H-4I). These data suggest that STAT1 is a critical regulator that mediates the function of the senescent GBM cell in immune microenvironment.

DDX58 regulated the protein stability of STAT1 via the ubiquitin E3 ligase TRIM21

Interestingly, DDX58 was also shown to be upregulated in senescent LN229 and U87MG cells (Figure S6A-S6B). When DDX58 was knocked down, the expression of STAT1 and phosphorylation were decreased (Figure 5A). Conversely, overexpression of DDX58 increased STAT1 and P21 expression (Figure 5B-5C). Therefore, we speculated that there may be a potential regulatory relationship between DDX58 and STAT1 in senescent cells. However, the inhibition of STAT1 did not affect *DDX58* mRNA expression (Figure S6C). Similarly, knockdown of DDX58 does not affect *STAT1* mRNA expression (Figure S6D). We subsequently used cycloheximide to inhibit protein translation after the knockdown of DDX58. The results indicated that the knockdown of DDX58 in TMZ-induced senescent LN229 cells accelerated STAT1 protein degradation (Figure 5D). Furthermore, after treatment with MG132, a proteasome inhibitor, the downregulation of the STAT1 protein caused by DDX58 knockdown in LN229 cells was rescued (Figure 5E). In addition, co-IP results indicated that DDX58 could bind endogenous STAT1 in LN229 cells (Figure 5F). TMZ treatment decreased the ubiquitin level of STAT1 in LN229 cells, whereas the opposite results were observed when DDX58 was knocked down in LN229 cells (Figure 5G). To further identify the mechanisms responsible for the ability of DDX58 to regulate STAT1 protein stability, we screened regulators of STAT1 ubiquitination, including USP22, USP39 and TRIM21.[31–33] We found that the TRIM21-STAT1 interaction was decreased through TMZ treatment (Figure 5H). DDX58 overexpression also reduced the binding of TRIM21 and STAT1 (Figure 5I). Hence, DDX58 promotes STAT1 protein stability, likely through suppressing the interaction between STAT1 and TRIM21. Moreover, UniProt database prediction revealed that the caspase recruitment domain (CARD), helicase domain and C-terminal regulatory domain (CTD) are the main functional domains of DDX58 (Figure 5J). To explore which domain of DDX58 plays a key role in the upregulation of the STAT1 protein, we transduced plasmids carrying various domains of DDX58 into LN229 glioma cells and human 293FT cells. Only the CARD of DDX58 obviously increased the protein level of STAT1 (Figure 5J). Furthermore, we performed functional verification of DDX58-overexpressing LN229 cells. CM from DDX58-overexpressing LN229 cells promoted the migration of THP-1 macrophages, and a similar effect was also observed after stimulation with 50 ng/mL recombinant human CSF1. In contrast, CM from DDX58-overexpressing LN229 cells treated with fludarabine decreased the migration of THP-1 macrophages (Figure 5K-5L). ELISA data and qPCR analysis further validated the increase in CSF1 in DDX58-overexpressing LN229 cells (Figure 5M and S6E). Furthermore, our data revealed that P21, NRF2 expression and the percentage of β-galactosidase-positive cells were decreased in STAT1-depleted plus DDX58-overexpressing glioma cells (Figure S6F-S6K). Together, these data indicate that activation of the DDX58-STAT1-CSF1 axis plays a vital role in GBM cell senescence and remodeling the immune microenvironment of GBM.

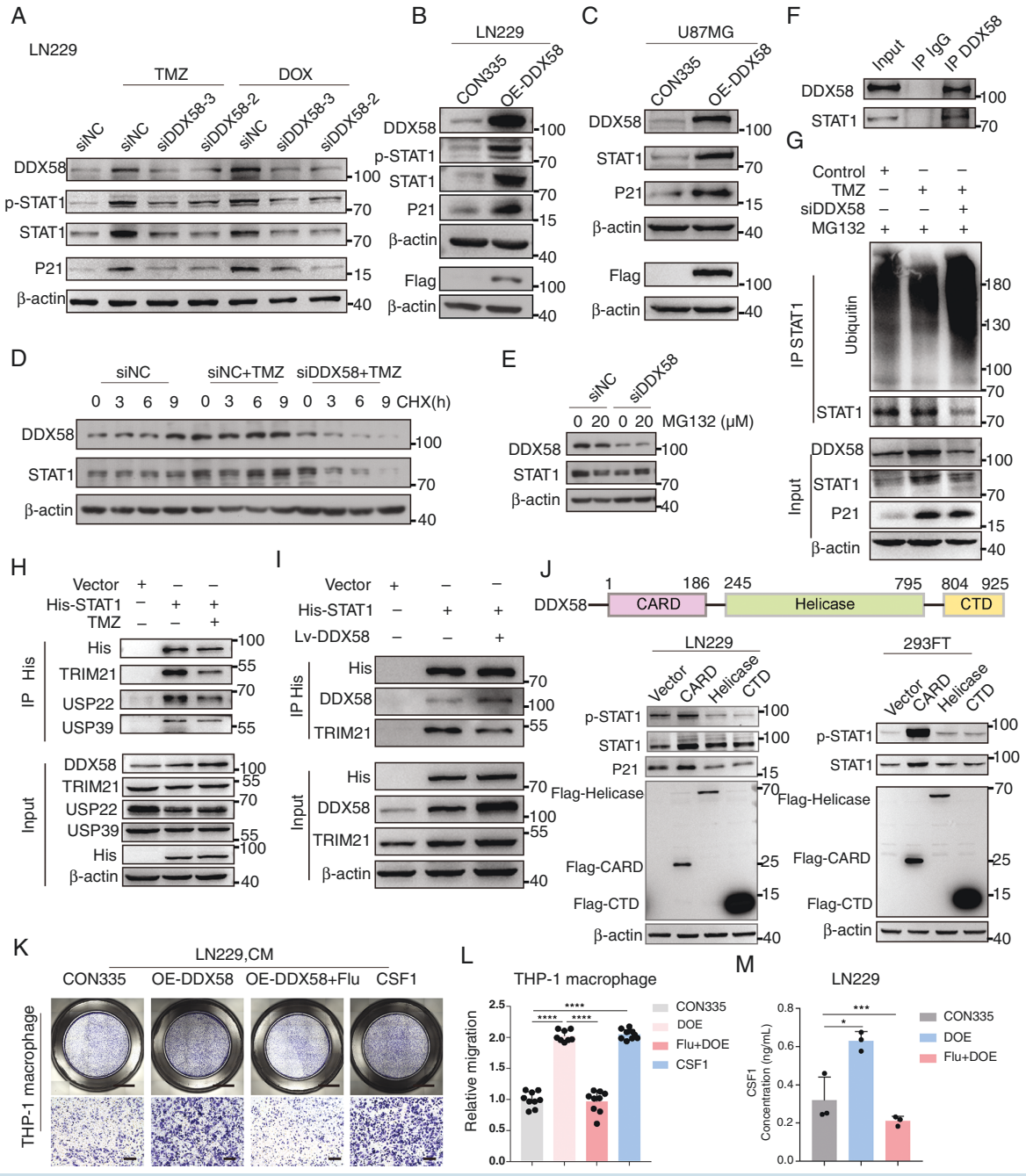

Figure 5. DDX58 regulated the protein stability of STAT1 via the ubiquitin E3 ligase TRIM21 (**A**). Western blot analysis of the DDX58, P21, and STAT1 proteins and their phosphorylation in DOX- or TMZ-induced senescent LN229 cells transduced with DDX58-targeting siRNAs. (**B-C**). Western blot analysis of the P21, DDX58, and STAT1 proteins and their phosphorylation in LN229 (B) and U87MG (C) cells overexpressing DDX58. (**D**). Protein stability assays to assess the effect of DDX58 on the STAT1 protein. DDX58-knockdown senescent LN229 cells were treated with cycloheximide (50 μg/mL) for up to 9 h, and STAT1 and DDX58 expression was tested via western blotting. (**E**). LN229 cells were transfected with DDX58 siRNA and then treated with MG132 (20 μM) for 5 h. (**F**). The binding between DDX58 and STAT1 was examined by co-IP and western blotting. (**G**). LN229 cells were transiently transfected with DDX58 siRNA and then treated with TMZ or DMSO, and the changes in the ubiquitin level of STAT1 in LN229 cells were examined by co-IP and western blotting. All the samples were treated with 20 μM MG132 for 2 h. (**H**). Regulators involved in the regulation of STAT1 ubiquitination were screened by transient transfection of LN229 cells with the His-STAT1 pcDNA 4.0 plasmid. One sample was treated with 50 μM TMZ for 4 days. All the cells were examined via co-IP and western blotting (**I**). LN229 cells were transiently transfected with the His-STAT1 plasmid, and changes in the STAT1 binding to TRIM21 in LN229 cells overexpressing DDX58 were examined via co-IP and western blotting. (**J**). Schematic diagram of the DDX58/RIG-I protein domains. P21 and STAT1 protein expression and phosphorylation by overexpressing the CARD, CTD, and helicase domains of DDX58 in LN229 and 293FT cells. (**K**). THP-1 macrophages were cocultured with CM from LN229 cells (CON335, DDX58 overexpressing, DDX58 overexpressing plus fludarabine, 50 ng/mL CSF-1) for 48 h. Scale bars: 1.5 mm, 150 μm. (**L**). Statistical analysis of the data in (K). The samples were analyzed in triplicate with 3 fields per well; $^{****}p < 0.0001$ by one-way ANOVA with Tukey's multiple comparison test. (**M**). ELISA analysis of CSF1 in LN229 cells overexpressing DDX58 or treated with fludarabine. Comparisons were performed with two-tailed Student's t tests. $^{*}p < 0.01$, $^{***}p < 0.001$. All the data are presented as the means ± SDs.

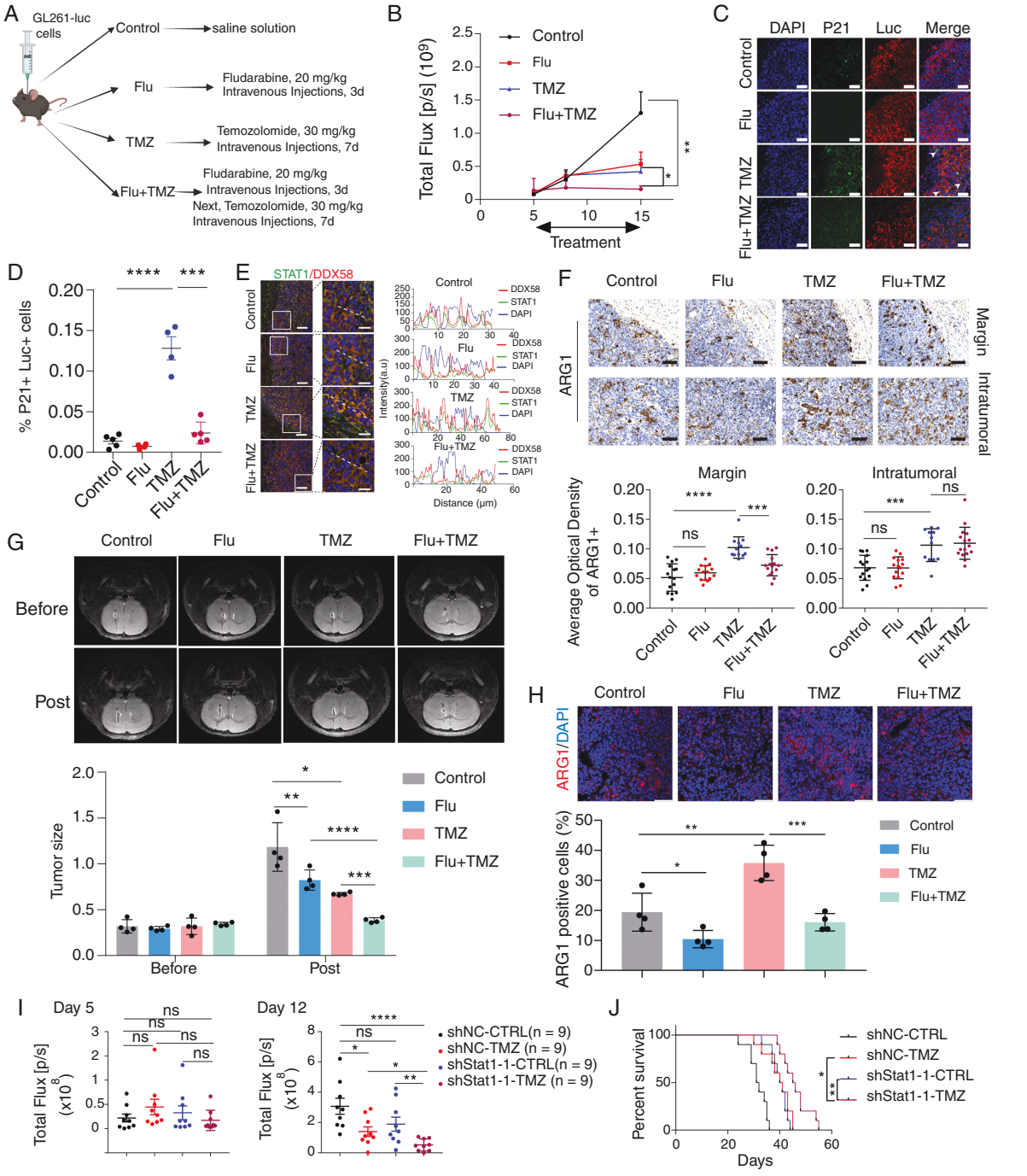

Figure 6. The combination of TMZ and fludarabine inhibited the growth of glioma in vivo (**A**). Schematic diagram of fludarabine combined with TMZ. Control: saline solution; Flu: fludarabine (20 mg/kg) for 3 days alone; TMZ: temozolomide (30 mg/kg) for 7 days; Flu + TMZ: 20 mg/kg fludarabine for 3 days followed by 20 mg/kg TMZ for 7 days. (**B**).Graph representing the integrated density over time from independent tumors. The data are presented as the means ± SEMs. *$p < 0.05$ and **$p < 0.01$ by one-way ANOVA with Tukey's multiple comparison test. (**C-D**). Representative images of P21 and luciferase staining in GL261-luc-derived tumors treated with fludarabine, TMZ, or both. The white arrows indicate P21 + senescent GL261 cells. Luc+/P21 + double-positive cells were quantified. ***$p < 0.001$ and ****$p < 0.0001$ by one-way ANOVA with Tukey's multiple comparison test. Scale bars: 40μm (**E**). Immunofluorescence and colocalization analysis of DDX58 and STAT1. DAPI staining was used to visualize the nuclei. Scale bars: 60μm, 20μm (**F**). Immunohistochemical staining and quantitative analysis of Arg1 show the M2-like macrophage (Arg1+) content. Scale bars, 50 μm. All the samples were analyzed in 3 fields per slice. The results are presented as the means ± SDs. ***$p < 0.001$ and ****$p < 0.0001$ by one-way ANOVA with Tukey's multiple comparison test.(**G**). MRI was performed to determine the tumor volume, and the statistical results are shown as the means ± SDs, *$p < 0.05$, **$p < 0.01$, ***$p < 0.001$ and ****$p < 0.0001$ by one-way ANOVA with Tukey's multiple comparison test. (**H**).Immunofluorescence staining and quantitative analysis of ARG1 content in PDX. Scale bars, 50 μm. The results are presented as the means ± SDs. *$p < 0.05$,**$p < 0.01$ and ***$p < 0.001$ by one-way ANOVA with Tukey's multiple comparison test. (**I**). Box and whisker plots representing the integrated density after 5 and 12 days. The data are presented as the means ± SEMs of n = 9 tumors

(shNC-CTRL), n = 9 tumors (shNC-TMZ), n = 9 tumors (shStat1-1-CTRL) and n = 9 tumors (shStat1-1-TMZ). *$p < 0.05$, **$p < 0.01$ and ****$p < 0.0001$ by one-way ANOVA with Tukey's multiple comparison test. (**J**). K–M survival curves of shNC-CTRL (n = 10, median survival 31.5 days) and shNC-TMZ (n = 10, median survival 40.5 days) mice treated with 20 mg/kg TMZ and K–M survival curves of Stat1-depleted GL261-derived tumor-bearing mice treated with saline (n = 10, median survival 40.5 days) or 20 mg/kg TMZ (n = 10, median survival 45.5 days), *$p < 0.05$ and **$p < 0.01$ according to the log-rank (Mantel–Cox) test.

TMZ treatment induced mitochondrial dsRNA accumulation in the cytoplasm

Moreover, it is not clear how the RNA-binding protein DDX58 is activated in therapy-induced senescent GBM cells. DDX58 recognises and binds to intracellular double-stranded RNA.[34] We speculated that the activation of DDX58 may be related to intracellular dsRNA. To test this hypothesis, we performed immune costaining of J2, an antibody used to detect dsRNA, and DDX58. The results revealed that the protein expression and cytoplasmic colocalization of dsRNA and DDX58 were increased in TMZ or DOX-induced senescent LN229 cells (Figure S7A-S7C). We also used a DDX58-agonist, 5′ppp-dsRNA, to activate the expression of DDX58 in LN229 cells. When DDX58 was activated, the expression of STAT1, p-STAT1 and P21 increased (Figure S7D). Immunoprecipitation with a J2 antibody revealed the binding of dsRNA and DDX58 in LN229 cells (Figure S7E). Delivery of the J2 antibody to senescent LN229 cells reduced the expression of DDX58 and STAT1, and the qPCR results revealed that the CSF1 mRNA level was decreased (Figure S7F-S7I). Interestingly, previous studies have shown that mitochondria may be a rich source of endogenous dsRNA.[35] During mitochondrial dysregulation, mitochondrial dsRNA can gain access to the cytosol via the Bcl2-associated X protein (Bax) and activate dsRNA sensors.[36] To further investigate dsRNA origin in senescent glioma cells, mitochondria were isolated from GBM cells (Figure S8A-S8B). The results revealed that TMZ or DOX treatment increased the expression of BAX in the mitochondria and cytoplasm (Figure S8A-S8B). RT–qPCR analysis revealed the accumulation of mitochondrial dsRNA (mtdsRNA) in the cytoplasm after TMZ or DOX treatment (Figure S8C-S8F). Moreover, these dsRNAs showed reduced colocalization with mitochondria in senescent GBM cells (Figure S8G-S8J). More importantly, BAX knockdown reduced the expression of DDX58 and STAT1 in the cytoplasm of senescent LN229 cells (Figure S8K). The accumulation of mtdsRNA in the cytoplasm was decreased in senescent LN229 cells with BAX knockdown (Figure S8L). These results suggest that the activation of DDX58 in senescent cells may be related to the cytoplasmic enrichment of mtdsRNA.

The combination of TMZ and fludarabine inhibited the growth of glioblastoma in vivo

We next analyzed whether the inhibition of STAT1 affected senescent malignant cells and reduced tumor growth in a GL261-derived GBM model (Figure 6A). Compared with TMZ treatment alone, combining fludarabine with TMZ effectively inhibited GBM growth (Figure 6B). After TMZ treatment alone, P21-positive GL261 cells were increased in the margins of the tumors. And the combination treatment reduced the number of P21-positive GL261 cells (Figure 6C-6D). Furthermore, the cytoplasmic colocalization of DDX58 and STAT1 was decreased in the marginal area of the combination-treated tumors (Figure 6E). ARG1 + macrophages were markedly decreased in the marginal area of the combination-treated tumors, but there was no significant change inside the tumors (Figure 6F). Furthermore, we utilized intracranial orthotopic PDX model to further evaluated the in vivo efficacy. Compared with TMZ treatment alone, combining fludarabine with TMZ effectively inhibited PDX growth (Figure 6G). $ARG1^+$ macrophages were markedly decreased in the combination-treated PDX tumors (Figure 6H).

We next assessed the impact of STAT1 depletion in GL261 cells on the progression of tumors in vivo. STAT1-depleted GL261-derived model mice treated with TMZ presented a lower proportion of CSF1-and ARG1-positive cells in tumor tissue (Figure S9A-S9B). Notably, the survival of glioblastoma-bearing mice harboring STAT1-depleted that were treated with TMZ was significantly greater than that of control mice treated with TMZ alone (Figure 6I-J). Moreover, to inhibit CSF-1 signaling in vivo, we used PLX3397, a small molecule that potently inhibits the tyrosine kinase activity of the CSF-1 receptor (CSF-1R) (Figure S9C). At 16 days, tumor size were smaller in mice receiving TMZ + PLX3397 treatment than in those receiving only TMZ or PLX3397 alone (Figure S9D). The proportion of CD68- and ARG1-positive cells were decreased after PLX3397 treatment (Figure S9E-S9F). Collectively, these data indicate that increased expression of DDX58 triggers the activation of STAT1 signaling, consequently facilitating the transcription of CSF1 in therapy-induced senescent GBM cells. This, in turn, results in the recruitment and polarization of TAMs, ultimately contributing to tumor progression and recurrence.

Discussion

Therapy-induced senescent cancer cells play both beneficial and detrimental roles during tumor progression depending on the context. Here, we report the tumor-promoting effect of therapy-induced senescent GBM cells in mouse models. These findings are consistent with recent studies showing that removal of malignant senescent cells improved the survival of GBM-bearing mice[23] and that radiation-induced SA-βGal + GBM cells contributed to tumor regrowth via active clonal expansion and global reorganization of the TME.[24] By coinjecting senescent GBM cells with tumorigenic cells, we provide more direct evidence for promoting tumor progression via therapy-induced senescent GBM cells. However, tumor growth was

promoted only when the relative proportion of senescent tumor cells reached a certain level (equal to the number of tumorigenic cells, Group 3 in Figure 2). A previous study also revealed that the use of twice as many senescent cells can promote tumor growth in vivo.[37] These findings suggest that the continued accumulation of senescent cells may lead to the malignant progression and regrowth of tumors in the TME.

By combining RNA sequencing and mass spectrometry, we observed the activation of STAT1 signaling in senescent LN229 cells. In TAMs, STAT1 shapes the metabolic program and drives the M1-like polarization of macrophages and antitumor responses.[38] Notably, glioma stem-like cells (GSCs) evade immune suppression through downregulation of STAT1 to initiate tumor growth, and STAT1 overexpression induces *p21* transcription and resensitizes GSCs to immune suppression.[39] In our study, the inhibition of STAT1 reduced the recruitment of macrophages by inhibiting *CSF1* transcription in senescent glioma cells. However, the number of ARG1 + macrophages (M2-like) markedly decreased in the marginal area of the tumors after the combination of fludarabine with TMZ, but there was no change inside the tumor. We speculated that a possible reason for this phenomenon is that fludarabine does not directly affect macrophages in vivo but rather inhibits marginally senescent tumor cells, which leads to a decrease in local macrophage recruitment in our model. This could be a novel immunomodulatory function of STAT1 in the GBM immune microenvironment. We also observed that the inhibition of STAT1 by fludarabine or siRNAs decreased SA-βGal activity and the expression of P21 in TMZ or DOX-treated GBM cells in vitro. Moreover, in the bone microenvironment, the suppression of Stat1 impedes osteoblast senescence and decreases the expression of SASPs, such as Ccl5 and Mmp9, which reduce age-related bone loss.[40] These findings revealed that STAT1 plays an important role in immune and senescence regulation in both pathological and physiological microenvironments.

DDX58 has previously been reported as an RNA-binding protein that regulates the stability of target mRNAs.[41,42] It has also been shown to be a mediator of SASPs.[43] However, we revealed that DDX58 regulates STAT1 at the post-translational level by inhibiting the degradation of the ubiquitin E3 ligase TRIM21-mediated STAT1. One possible reason for the activation of DDX58 is the enrichment of intracellular dsRNA. In the antiviral immune response, DDX58 recognizes viral dsRNA and then activates the type-I interferon response, leading to the rapid induction of cytokines.[44,45] Here, we showed that the cytoplasmic colocalization of dsRNA and DDX58 was increased in senescent cells. Cellular senescence is closely related to mitochondrial dysfunction.[46,47] Mitochondrial damage promotes mtdsRNA efflux, activating DDX58-mediated innate immune response in cellular senescence.[48]Moreover, In the antiviral response, the BAX protein mediates the release of mtdsRNA into the cytoplasm.[36] Interestingly, we found that the expression of the BAX protein was elevated in the mitochondria, and mtdsRNA was also increased in the cytoplasm under TMZ or DOX treatment. Together, our results and those of previous studies suggest that the mtdsRNA may be the main cause of DDX58-STAT1-CSF1 axis activation in therapy-induced senescent GBM cells. It also reveals a key mechanism by which senescent GBM cells mediate TAMs infiltration. It is worth noting that the DDX58-STAT1 signaling may have certain associations and complementarities with the previously reported roles of NRF2 and HGF. NRF2 activity determines malignant cell senescent phenotype in primary GBM.[23] Knockdown of STAT1 in DDX58 overexpressing cells decreased NRF2 expression. This suggests that NRF2 may be a downstream factor for the DDX58-STAT1 axis to regulate GBM senescence. And HGF can contribute to the SASP in senescent GBM cells by acting on neighboring cells, which may facilitate tumor radioresistance and recurrence.[24,49] We observed an elevation in EGF expression in GBM cells overexpressing DDX58, yet this upregulation was independent of STAT1. So, DDX58 may directly influence the secretion of HGF and modulate its effects on senescent GBM cells.

To assess whether STAT1-mediated inhibition of senescence also has potential for clinical-related applications in vivo, a combination treatment approach was proposed. However, unlike the common strategy of first inducing cancer senescence and then eliminating senescent cancer cells,[50] our strategy is to first pretreat cancer cells with a STAT1 inhibitor or depleted STAT1 and then treat them with TMZ, which can also achieve the effect of combination therapy. Compared with fludarabine or TMZ treatment alone, pretreatment with fludarabine followed by TMZ therapy inhibited GBM growth in intracranial tumor models. The median survival of GBM-bearing mice harboring STAT1-depleted that were treated with TMZ was significantly greater than that of control mice. Although, the efficacy of STAT1 knockout could not be visible additive with TMZ on the overall survival time. Studies have demonstrated that STAT1 also mediates alterations in tumor immunogenicity.[51] By knocking down STAT1, it is possible to decrease the immunogenicity of tumor cells and impede the cytotoxic activity of T cells against tumor cells in vivo. This suggests that the therapeutic efficacy of STAT1 inhibition may be intimately linked to tumor immune escape mechanisms, the tumor microenvironment, and the adaptive mechanisms of tumor cells. Consequently, optimizing treatment strategies and addressing immune escape remain key areas of focus for future research. Moreover, A clinical study demonstrated that PLX3397 (pexidartinib) treatment induced systemic CSF1 upregulation and reduced $CD14^{dim}CD16^{+}$ monocyte levels in patients, confirming its CSF1R-inhibitory activity.[52] However, unlike these systemic effects, no significant CSF1 elevation was detected in the tumor microenvironment (TME) of PLX3397-treated male mice. This discrepancy highlights potential interspecies differences in drug response and translational mechanisms. Future studies should investigate how systemic CSF1R inhibition modulates the TME to optimize the clinical utility of PLX3397.

Our data collectively support the previously unidentified concept that activation of the DDX58-STAT1-CSF1 signaling axis during TIS is a central initiator that remodels the TME for GBM treatment and recurrence. This information may be critical for advancing therapeutic strategies. However, many important issues remain to be solved, such as how to minimize toxic side-effects. Therefore, the discovery of new drugs that target cellular senescence is necessary.

Supplementary material

Supplementary material is available online at *Neuro-Oncology* (https://academic.oup.com/neuro-oncology).

Keywords

Glioblastoma | Senescence | TAM | Immune microenvironment | DDX58 | STAT1

Abbreviations:

CM: conditioned media; mtdsRNA: mitochondrial double-stranded RNA; TAMs: tumor-associated macrophages; GBM: Glioblastoma; STCs: senescent tumor cells; SASP: senescence-associated secretory phenotype; TIS: therapy-induced senescence; TME: tumor microenvironment; TMZ: temozolomide; DOX: Doxorubicin; ELISA: Enzyme-linked immunosorbent assay; CSF1: colony stimulating factor-1; RBPs: RNA-binding proteins

Funding

This work was supported by the National Key R&D Program of China (2022YFC3401002, 2022YFA1103803), the CAMS Innovation Fund for Medical Sciences (CIFMS) grant (2021-I2M-1–034), Brain Tumor Precision Diagnosis and Treatment and Translational Medicine Innovation Unit, Chinese Academy of Medical Sciences (2019-I2M-5-021), the National Natural Science Foundation of China (82173373, 82002994, 81761168038), and State Key Laboratory Special Fund 2060204.

Acknowledgements

We thank State Key Laboratory of Common Mechanism Research of Major Diseases Platform for consultation and instrument availability that supported this work. The graphical abstract was created using BioRender.com.

Author contributions

Zhixing Wang: Conceptualization, Investigation, Methodology, Writing–original draft.Yuxin Zhang: Methodology, Writing – review & editing. Fan Wu: Methodology, Data analysis, Funding acquisition. Bojun Qiu: Methodology, review & editing. Xinrun Wang: Methodology, review & editing. Xin Zhang: Methodology, review & editing. Wanjun Tang: Methodology, review & editing. Zefan Jing: review & editing. Yiyun Yin, Ruoyu Huang and Zhiyan Sun: Collection of clinical samples and data. Wei Han: Supervision, Conceptualization, Funding acquisition, Writing – review & editing. Tao Jiang: Supervision, Conceptualization, Funding acquisition, Writing – review & editing Xiaozhong Peng: Supervision, Conceptualization, Funding acquisition Writing – review & editing.

Conflict of Interest

The authors declare no competing interests.

Affiliations

State Key Laboratory of Common Mechanism Research for Major Diseases, Department of Biochemistry & Molecular Biology, Medical Primate Research Center, Neuroscience Center, Institute of Basic Medical Sciences Chinese Academy of Medical Sciences, School of Basic Medicine Peking Union Medical College, Beijing 100005, China. (Z.W., Y.Z., B.Q., X.W., X.Z., W.T., Z.J., W.H., X.P.) ; Department of Molecular Neuropathology, Beijing Neurosurgical Institute, Capital Medical University, Beijing, 100070, China. (F.W., Y.Y., R.H., Z.S.,T.J.) ; Department of Neurosurgery, Beijing Tiantan Hospital, Capital Medical University, Beijing, 100070, China. (F.W., Y.Y., R.H., Z.S.,T.J.); State Key Laboratory of Respiratory Health and Multimorbidity, Beijing 100005, China. (X.P.); Institute of Laboratory Animal Science, Chinese Academy of Medical Sciences & Peking Union Medical College, Beijing, 100021, China. (X.P.)

References

1. Stupp R, Mason WP, van den Bent MJ, et al. Radiotherapy plus concomitant and adjuvant temozolomide for glioblastoma. *Cancer/Radiothérapie.* 2005;9(3):196–197.
2. McLendon RE, Hjelmeland AB, Dewhirst MW, et al. Glioma stem cells promote radioresistance by preferential activation of the DNA damage response. *Nature.* 2006;444(7120):756–760.
3. Almog N, Ma L, Abdollahi A, et al. Transcriptional switch of dormant tumors to fast-growing angiogenic phenotype. *Cancer Res.* 2009;69(3):836–844.
4. Patel AP, Tirosh I, Trombetta JJ, et al. Single-cell RNA-seq highlights intratumoral heterogeneity in primary glioblastoma. *Science.* 2014;344(6190):1396–1401.
5. Barker HE, Paget JT, Khan AA, Harrington KJ. The tumour microenvironment after radiotherapy: mechanisms of resistance and recurrence. *Nat Rev Cancer.* 2015;15(7):409–425.
6. Rusu P, Shao C, Neuerburg A, et al. GPD1 specifically marks dormant glioma stem cells with a distinct metabolic profile. *Cell Stem Cell.* 2019;25(2):241–257.e8.
7. Sampson JH, Gunn MD, Fecci PE. Brain immunology and immunotherapy in brain tumours. *Nat Rev Cancer.* 2020;20(1):12–15.
8. Xuan W, Lesniak MS, James CD, Heimberger AB, Chen P. Context-dependent glioblastoma–macrophage/microglia symbiosis and associated mechanisms. *Trends Immunol.* 2021;42(4):280–292.
9. Fernando O Martinez SG. The M1 and M2 paradigm of macrophage activation: time for reassessment Fernando O. Martinez1* and Siamon Gordon2. *F1000Prime Rep.* 2014;6(3):6–13.

10. Cheng N, Bai X, Shu Y, Ahmad O, Shen P. Targeting tumor-associated macrophages as an antitumor strategy. *Biochem Pharmacol.* 2021;183(2021):114354.
11. Mantovani A, Sica A, Sozzani S, et al. The chemokine system in diverse forms of macrophage activation and polarization. *Trends Immunol.* 2004;25(12):677–686.
12. Gong D, Shi W, Yi S, et al. TGFβ signaling plays a critical role in promoting alternative macrophage activation. *BMC Immunol.* 2012;13(1):31.
13. Hambardzumyan D, Gutmann DH, Kettenmann H. The role of microglia and macrophages in glioma maintenance and progression. *Nat Neurosci.* 2016;19(1):20–27.
14. Wu M, Wu L, Wu W, et al. Phagocytosis of glioma cells enhances the immunosuppressive phenotype of bone marrow-derived macrophages. *Cancer Res.* 2023;83(5):771–785.
15. Chien Y, Scuoppo C, Wang X, et al. Control of the senescence-associated secretory phenotype by NF-kappaB promotes senescence and enhances chemosensitivity. *Genes Dev.* 2011;25(20):2125–2136.
16. Kansara M, Leong HS, Lin DM, et al. Immune response to RB1-regulated senescence limits radiation-induced osteosarcoma formation. *J Clin Invest.* 2013;123(12):5351–5360.
17. Chanhee K, Xu Q, Martin TD, et al. The DNA damage response induces inflammation and senescence by inhibiting autophagy of GATA4. *Science.* 2015;349(6255):aaa5612.
18. Kim YH, Choi YW, Lee J, et al. Senescent tumor cells lead the collective invasion in thyroid cancer. *Nat Commun.* 2017;10(8):15208.
19. Choi YW, Kim YH, Oh SY, et al. Senescent tumor cells build a cytokine shield in colorectal cancer. *Adv Sci.* 2021;8(4):2002497.
20. Chen HA, Ho YJ, Mezzadra R, et al. Senescence rewires microenvironment sensing to facilitate antitumor immunity. *Cancer Discov.* 2023;13(2):432–453.
21. Hanna A, Balko JM. No rest for the wicked: tumor cell senescence reshapes the immune microenvironment. *Cancer Cell.* 2023;41(5):831–833.
22. Wang L, Lankhorst L, Bernards R. Exploiting senescence for the treatment of cancer. *Nat Rev Cancer.* 2022;22(6):340–355.
23. Salam R, Saliou A, Bielle F, et al. Cellular senescence in malignant cells promotes tumor progression in mouse and patient Glioblastoma. *Nat Commun.* 2023;14(1):441.
24. Jeon H, Kim J, Cho HJ, et al. Tissue factor is a critical regulator of radiation therapy-induced glioblastoma remodeling. *Cancer Cell.* 2023;41(8):1480–1497.e9.
25. Xie XP, Laks DR, Sun D, et al. Quiescent human glioblastoma cancer stem cells drive tumor initiation, expansion, and recurrence following chemotherapy. *Dev Cell.* 2022;57(1):32–46.e8.
26. Yabo YA, Moreno-Sanchez PM, Pires-Afonso Y, et al. Glioblastoma-instructed microglia transition to heterogeneous phenotypic states with phagocytic and dendritic cell-like features in patient tumors and patient-derived orthotopic xenografts. *Genome Med.* 2024;16(1):51.
27. Zhang L, Pitcher LE, Yousefzadeh MJ, et al. Cellular senescence: a key therapeutic target in aging and diseases. *J Clin Invest.* 2022;132(15):e158450.
28. Varesi A, Campagnoli L, Barbieri A, et al. RNA binding proteins in senescence: a potential common linker for age-related diseases? *Ageing Res Rev.* 2023;88(2023):101958.
29. Tesei A, Arienti C, Bossi G, et al. TP53 drives abscopal effect by secretion of senescence-associated molecular signals in non-small cell lung cancer. *J Exp Clin Cancer Res.* 2021;40(1):89.
30. Pyonteck SM, Akkari L, Schuhmacher AJ, et al. CSF-1R inhibition alters macrophage polarization and blocks glioma progression. *Nat Med.* 2013;19(10):1264–1272.
31. Peng Y, Guo J, Sun T, et al. USP39 serves as a deubiquitinase to stabilize STAT1 and sustains type I IFN-induced antiviral immunity. *J Immunol.* 2020;205(11):3167–3178.
32. Li M, Xu Y, Liang J, et al. USP22 deficiency in melanoma mediates resistance to T cells through IFNgamma-JAK1-STAT1 signal axis. *Mol Ther.* 2021;29(6):2108–2120.
33. Zhang L, Li Q, Yang J. Cytosolic TGM2 promotes malignant progression in gastric cancer by suppressing the TRIM21-mediated ubiquitination/degradation of STAT1 in a GTP binding-dependent modality. *Cancer Commun.* 2023;43(1):123–149.
34. Onomoto K, Onoguchi K, Yoneyama M. Regulation of RIG-I-like receptor-mediated signaling: interaction between host and viral factors. *Cell Mol Immunol.* 2021;18(3):539–555.
35. Chen YG, Hur S. Cellular origins of dsRNA, their recognition and consequences. *Nat Rev Mol Cell Biol.* 2022;23(4):286–301.
36. Dhir A, Dhir S, Borowski LS, et al. Mitochondrial double-stranded RNA triggers antiviral signalling in humans. *Nature.* 2018;560(7717):238–242.
37. Omer A, Barrera MC, Moran JL, et al. G3BP1 controls the senescence-associated secretome and its impact on cancer progression. *Nat Commun.* 2020;11(1):4915–4979.
38. Huffaker TB, Ekiz HA, Barba C, et al. A Stat1 bound enhancer promotes Nampt expression and function within tumor associated macrophages. *Nat Commun.* 2021;12(1):2620.
39. Zhan X, Guo S, Li Y, et al. Glioma stem-like cells evade interferon suppression through MBD3/NuRD complex-mediated STAT1 downregulation. *J Exp Med.* 2020;217(5):e20191340.
40. Xu JZ, Zhou YM, Zhang LL. BMP9 reduces age-related bone loss in mice by inhibiting osteoblast senescence through Smad1-Stat1-P21 axis. *Cell Death Discovery.* 2022;8(1):330.
41. MacNair L, Xiao S, Miletic D, et al. MTHFSD and DDX58 are novel RNA-binding proteins abnormally regulated in amyotrophic lateral sclerosis. *Brain.* 2016;139(Pt 1):86–100.
42. Wu S-F. LXAX. RIG-I regulates myeloid differentiation by promoting TRIM25-mediated ISGylation. *Proc Natl Acad Sci U S A.* 2020;117(25):14395–14404.
43. Liu F, Wu S, Ren H, Gu J. Klotho suppresses RIG-I-mediated senescence-associated inflammation. *Nat Cell Biol.* 2011;13(3):254–262.
44. Kato H, Takeuchi O, Sato S, et al. Differential roles of MDA5 and RIG-I helicases in the recognition of RNA viruses. *Nature.* 2006;441(7089):101–105.
45. Peisley A, Wu B, Yao H, Walz T, Hur S. RIG-I forms signaling-competent filaments in an ATP-dependent, ubiquitin-independent manner. *Mol Cell.* 2013;51(5):573–583.
46. Wiley CD, Velarde MC, Lecot P, et al. Mitochondrial dysfunction induces senescence with a distinct secretory phenotype. *Cell Metab.* 2016;23(2):303–314.
47. Miwa S, Kashyap S, Chini E, von Zglinicki T. Mitochondrial dysfunction in cell senescence and aging. *J Clin Invest.* 2022;132(13):1–9.
48. Kim S, Lee K, Choi YS, et al. Mitochondrial double-stranded RNAs govern the stress response in chondrocytes to promote osteoarthritis development. *Cell Rep.* 2022;40(6):111178.
49. Fletcher-Sananikone E, Kanji S, Tomimatsu N, et al. Elimination of radiation-induced senescence in the brain tumor microenvironment attenuates glioblastoma recurrence. *Cancer Res.* 2021;81(23):5935–5947.
50. Li F, Liu P, Mi W, et al. Blocking methionine catabolism induces senescence and confers vulnerability to GSK3 inhibition in liver cancer. *Nat Cancer.* 2024;5(1):131–146.
51. Lv J, Zhou Y, Zhou N et al.. Epigenetic modification of CSDE1 locus dictates immune recognition of nascent tumorigenic cells. *Sci Transl Med.* 2023;15(681):eabq6024.
52. Mendez JS, Cohen AL, Eckenstein M, et al. Phase 1b/2 study of orally administered pexidartinib in combination with radiation therapy and temozolomide in patients with newly diagnosed glioblastoma. *Neurooncol. Adv.* 2024;6(1):vdae202.